Thermochemistry of Ruthenium in Molten Fluoride Salts

Metal or Melt?

by
Laurens G. Braskamp

in partial fulfillment of the requirements
for the degree of

Bachelor of Science
in
Molecular Science and Technology
at the
Delft University of Technology

to be defended publicly
on Monday, August 20, 2018
at 14:30

Student numbers: **4411064 (TU Delft)**
1517988 (Universiteit Leiden)

Thesis Committee: **dr. Elisa Capelli (supervisor)**
TU Delft **dr. Anna L. Smith**
prof. dr. Rudy J.M. Konings

Abstract

The Molten Salt Reactor (MSR) is a member of safer and more sustainable fourth generation of nuclear reactors, the development of the might be crucial to continually secure supply of electrical energy from the near future onwards. Because the fluorides of ruthenium ($_{44}$Ru) are a poorly investigated group of fission products that might be born during MSR operation, some computational research was done on their thermochemistry.

Because little experimental data on these species has been obtained, the gas-phase molecular geometries and formation enthalpies of all known Ru-F binary compounds, RuF, RuF_2, RuF_3, RuF_4, RuF_5, RuF_6, $(RuF_5)_2$ and $(RuF_5)_3$ are calculated by Density Functional Theory. The DFT/B3LYP method was employed with quasi-relativistic ECP28MWB pseudopotentials and basis set on ruthenium and cc-pVTZ basis set on fluorine. Standard molar entropies and heat capacities were then also calculated by statistical mechanics computations.
From the obtained thermochemical data, part of which had to be optimized, and additional data on the solid and liquid phases, the Ru-F subsystem was assessed using the CALPHAD methodology. Based on the developed model, a phase diagram, Ellingham diagram and gas-phase equilibrium diagram were calculated. These diagrams serve as a first attempt to describe and predict the behavior of ruthenium in the reactor core during operation of the MSR.

It was found that, assuming that the calculated parameters correctly represent the Ru-F subsystem, ruthenium prefers to be in its metallic solid state under MSR operation conditions. Generation of more experimental thermochemical data on ruthenium fluorides is desired to confirm or correct the data obtained from the computations, in order to eventually be able to commercially operate MSRs for future electricity generation.

Preface

Finally.

That's what this thesis project can best be described and summarized with. It took me several more months than I initially planned. Those past months have, though, been a fruitful time.
This year, I learned many things. Many things about nuclear science, the topic of this my thesis. About chemistry, my field of study. I had a most interesting and informative time at the Reactor Institute of the Delft University of Technology. I'll be thankful to its staff and people for my life to come, for the opportunities I was given.
Many things I learned too about myself. About planning and sticking to it. About organizing and wasting time. About my attitude to work and my true passions in life. About my apparently irrepressible need for both sleep and schedule. It has been a fruitful time.

Finally, I feel the need to express my gratitude especially and explicitly to anyone who has been a help to me on the way hitherto. Thanks be to my supervisor, Elisa, as well as to her colleagues at and the staff of the Reactor Physics and Nuclear Materials section, of whom the secretary in particular. Thanks also to the academic counsellor, and the guidance from Stumass.
Deo autem ante omnibus gratias.

Laurens G. Braskamp
Delft, July 2018

Table of contents

1. Introduction

1.1. Nuclear Energy Generation

The principle of nuclear energy generation is basically expressed by Einstein's famous formula

$$E = mc^2 \quad \textbf{(1)}$$

stating that mass essentially is an appearance of energy. Conversion of mass-energy to other forms of energy (such as heat, work, or electricity) is implied possible by application of the First Law of Thermodynamics, and the technology involved to facilitate the generation of nuclear power has been developed over a hundred years.

In contrast with today's main (fossil) energy sources, such as oil, natural gas and coal, the generation process of nuclear power produces no CO_2. Therefore, it is a promising candidate to be a solid and reliable basis of future energy supply. Its only emission sources are fuel pre- and post-processing, as well as facility construction, the latter of which, although often neglected, is also non-zero for devices like solar panels and wind turbines.

Although the energy generation process itself thus is climate neutral, nuclear energy is not widely considered 'green'. This might be because, in contrast to well-known sustainable energy sources as solar, wind, and hydropower, nuclear fuel is mined and processed, just like fossil fuels. Also, the fact that highly radiotoxic waste is left at the end of the process contributes to the generally negative public attitude towards nuclear power.

Public opinion on nuclear energy is highly affected by three incidents. In 1979, control was lost over one of the reactors at Three Mile Island, PA. Although only little radioactive material escaped, this accident initiated the anti-nuclear movement.
Seven years later, the infamous Chernobyl accident occurred. It released radioactive materials over nearly all of Europe, and the area around the reactor complex will be too toxic to inhabit for ages. After the Chernobyl disaster, various nuclear power plants in Europe were decommissioned – some of which were not even built yet – and only few reactors have been built since [1].
More recently, a tsunami after an earthquake knocked out the Fukushima nuclear power plant, which lost a significant amount of radioactive material and set Japan too to think about the safety of their nuclear reactors. Likely, the exact consequences of this latest accident cannot be determined yet.

Fortunately, these accidents have not stopped research into nuclear reactors, and the current, fourth generation of nuclear reactors is being developed thoroughly to achieve safer designs and less production of lower-radiotoxic waste. Among these Gen-IV reactor concepts, the one which the research reported here applies to, is the Molten Salt Reactor.

1.2. The Molten Salt Reactor (MSR) [2]

The concept of the Molten Salt Reactor (MSR) is not completely new. Already from 1957 onwards, in the very childhood of nuclear power, the US Atomic Energy Commission ran a small MSR experiment at the Oak Ridge National Laboratory (ORNL) in Tennessee [3]. The experimental reactor operated in 1965-68 on ^{235}U fuel and was in 1968-69 the first-ever nuclear reactor using the ^{232}Th/^{233}U fuel cycle; after completion of all experiments, it was shut down [3, pp. 10-13].

The most distinctive MSR feature is the use of liquid-state fuel instead of the solid fuel rods usually employed to date. This fuel fluid consists of one or several actinide fluorides (such as UF_4 and ThF_4) dissolved in a molten fluoride salt, which can contain various salts like LiF, BeF_2, and ZrF_4. These nuclei have small neutron-capture cross sections, so that they virtually do not interfere with the nuclear chain reaction. As a moderator, graphite is commonly used.

The MSR is operated at ambient pressure (which annihilates the risk of explosion) and temperatures around 900 K. Because nuclear fission also generates heat, the reactor is cooled with a second molten salt circuit, also containing fluoride salts like LiF-BeF_2 (FLiBe) or NaF-$NaBF_4$. The main reason why MSRs are inherently safer than the nuclear reactors in commercial use, besides the ambient pressure, is the fact that the MSR temperature and void coefficients of reactivity are negative. This means that in case of a sudden power increase, the MSR core does not run away, but levels off its power output.

1.3. Fission Products in MSRs [3]

As uranium fission occurs in the molten salt, its fission products will be produced therein. Highly volatile fission products, such as xenon and krypton isotopes, are likely to come out of the fluid, assisted by helium bubbling. Most elements, including iodine, bromine, rubidium, cesium and all lanthanides, form stable fluoride salts that dissolve in the salt mixture. The class of fission products that needs most attention is the group of noble metals, such as niobium, molybdenum, silver, and ruthenium. These metals are expected to form solid precipitates and therefore accumulate in the mixture, settling on various surfaces and thereby forming obstacles in the energy production process. For good operation of a MSR, fission product behavior must be understood [3, p. 2].

Most uranium fission products themselves are also radioactive, and most of them (including the abovementioned ruthenium isotopes) will disintegrate by beta decay. Moreover, the average oxidation state of the metals in the mixture changes; uranium (or thorium) is fed as U^{4+}/Th^{4+}, while the average oxidation state of the fission products is around +3 [4]. As a result of the production of fission products of lower oxidation state and of beta particles (physically equal to electrons), the electronic status of the reactor contents, known as redox potential, is changing over time. When this potential increases enough, even the most noble metals will be oxidized and form salts, blending in the melt. Likely, most of these salts will be fluoride salts, as the fluoride anion is amply present as constituent of the feed salt mixture. Different anions are formed in the reactor processes, like iodide or bromide, perhaps even selenium or tellurium anions, but these are not abundant in the reactor contents. Thus, the redox condition of the MSR contents is described by the fluorine potential [5]:

$$\Delta\overline{G}_{F_2} \equiv RT \ln p_{F_2} \qquad \textbf{(2)}$$

with R the gas constant, T the temperature and p_{F_2} the partial pressure of gaseous fluorine. This fluorine potential is usually controlled by addition of some UF_3 to the fuel salt. By effective and efficient fluorine potential management, operators know what are the chemical forms and states of the reactor contents, and are able to know them also in case of an accident.

Typically, the fluorine potential in a MSR is about $\Delta\overline{G}_{F_2} \cong -700$ kJ/mol. This can be calculated by the dissolved-salt control formula (15) from [5, p. 271], assuming a U^{4+}/U^{3+} ratio of 100 [3, p. 15] and using the Gibbs energies of formation for UF_4 and UF_3 dissolved in FLiBe as reported in the report ORNL-4076 [6, p. 49], which are given in kcal/mol.

Of the noble metals, a considerable, yet poorly investigated portion is ruthenium, in particular the isotopes ^{103}Ru and ^{106}Ru [3, pp. 17, 19-90]. Both will decay further, but their reasonably long half-life periods (of 39.26 days and 373.59 days respectively) make them to be considered. In fact, after the ORNL experimental MSR shut down, substantial amounts of ruthenium were found all over the reactor inventory [3, pp. 91-134].

1.4. Research Aim

Combining the aforementioned considerations, the research reported here attempts to calculate the behavior of ruthenium as it depends on the system temperature and fluorine potential. After investigation what binary species of ruthenium fluorides are found to exist, the thermochemical properties of these are computed combining DFT and statistical mechanics calculations. As a result, a phase diagram is to be presented showing the thermodynamically expected behavior of ruthenium in a MSR environment.

2. Literature Review

Various ruthenium fluorides are known to exist, although little research has been investigating their thermochemical behavior under high-temperature MSR conditions.

A 1987 thesis mentions the existence and synthesis methods of five binary ruthenium-fluorine compounds: RuF_3, RuF_4, RuF_5, RuF_6 and RuF_8, alongside with mono-, di- and trivalent anions of RuF_6 [7]. The hexa- and octafluoride are reported to be thermally unstable: whereas the former has a distinct red-brown vapor and a decomposition temperature around 200 °C [8], the latter already decomposes at –50 °C [7]. Ruthenium octafluoride has not been mentioned in literature ever since, and is therefore not included in this work.
The following year, the gaseous lower ruthenium fluorides (RuF and RuF_2) are found in literature [9], and five years later, the RuF_5 gas phase is observed to consist of mainly trimeric molecules in two different, non-planar conformations, as well as some dimeric molecules [10]. Several values for the formation enthalpies, bond dissociation energies, molecular bond lengths and symmetries for gaseous ruthenium fluorides are shown in Table 1. In addition to the symmetry point groups listed there, the pentafluoride is already known to prefer the square pyramidal C_{4v} structure over the trigonal bipyramidal D_{3h}, and the tetrafluoride is reported to be more stable in square planar D_{4h} conformation than in the initially expected tetrahedron T_d [11], [12].

Table 1: Standard Enthalpy of Formation ΔH_f^0, bond dissociation energies D_e, bond lengths and point groups of the gaseous ruthenium fluorides found in literature. Here and henceforth, (ax) refers to bonds from a central (ruthenium) to an axial positioned atom, (eq) to a bond in the equatorial plane, and (b) to a bond to a bridging (Ru-F-Ru) atom.

	ΔH_f^0 (kJ/mol)	D_e (kJ/mol)	Bond lengths (Å)	Point Group	Ref.
RuF	328.4	402			[9]
	271.2				[13]
		364.8	2.05	$C_{\infty v}$	[11], [14]
RuF_2	–55.2	464			[9]
	–130.3				[13]
		508.4	1.96	$D_{\infty h}$	[11], [15]
RuF_3	–314.2	339			[9]
	–390.3				[13]
RuF_4	–595.0	361			[9]
	–646.0				[13]
			1.87	T_d	[16]
RuF_5	–740.5				[13]
	–744.8		1.87	D_{3h}	[16]
RuF_6	–848.3				[13]
			1.8775	O_h	[16]
			1.8467 (ax), 1.8204 (eq)	D_{4h}	[17]
$(RuF_5)_2$	–1686.2				[13]
$(RuF_5)_3$	–2600.5				[13]
			2.00 (b), 1.85 (ax), 1.77 (eq)	C_{3v}, C_S	[10], [11]

The often serious differences between obtained numbers arise usually from the approach elected to calculate the desired value. Siegbahn (in [14], [15]) calculates the properties of the bonding in second-row transition metal (di-)fluorides in correlation with their (di-)hydrides and (di-)chlorides. Hildebrand and Lau [9] used some figures from neighboring molybdenum (*Z=42*; for Ru, *Z=44*) to fill knowledge gaps to calculate formation enthalpies from enthalpies of reactions involving ruthenium and silver fluorides, whereas Nikitin and Zbezheva [13] only use mutual equilibrium reactions amongst the ruthenium fluorides themselves and calibrate these relative values with a literature value measured by bomb calorimetry [18]. This measured value for solid ruthenium pentafluoride is reported to be ΔH_f^0(RuF_5, (s)) = –892.9 kJ/mol. Data on the condensed phases of all other ruthenium fluorides appear to be scarce, if not non-existent.

Clearly, there is an enormous lack of data on the majority of ruthenium fluoride species. Part of the information that is available is not even calculated, but estimated; thermochemical data usually is not even available. Therefore, the thermodynamics of the mentioned ruthenium fluorides are to be computed again, while the literature serves as a reference background to judge the reasonability of the newly calculated values – the only exception is the mentioned measured value for RuF_5 (s).

3. Theoretical Background

3.1. Density Functional Theory (DFT)

Density Functional Theory is an *ab initio* quantum mechanical approach to calculating molecular geometries and properties, which simplifies the Hamiltonian of the Schrödinger equation by considering all individual electrons as one 'cloud' of time-averaged electron density. Nowadays, it is one of the most used tools in computational chemistry. It is capable of computing all molecular properties quite accurately with reasonable effort [19].

First of all, there are multiple ways to calculate molecular energetics from DFT, called methods. The one method that was used in this work is called B3LYP [20], one of today's most used and most accurate methods [19, pp. 266-98]. It is an Adiabatic Connection Method (ACM), the mentioned 'connection' being made between the Kohn-Sham (KS) system, in which electrons do not interact with each other, and the actually interactive system. The correction thus carried out is commonly denoted as *exchange-correlation energy* (E_{XC}), which is included in the energetic expression following from the KS Self-Consistent Field (SCF) methodology [19, pp. 255-57].

The main output of the DFT calculations is the molecular geometry (represented in vector $\vec{\boldsymbol{r}}$), which all molecular properties depend on. It is computed by minimizing the energy functional

$$E[\rho(\vec{\boldsymbol{r}})] = T_{nuc,i}[\rho(\vec{\boldsymbol{r}})] + V_{nuc-el}[\rho(\vec{\boldsymbol{r}})] + V_{el-el}[\rho(\vec{\boldsymbol{r}})] + \Delta T[\rho(\vec{\boldsymbol{r}})] + \Delta V_{el-el}[\rho(\vec{\boldsymbol{r}})] \quad \textbf{(3)}$$

where the terms T are kinetic energy functionals and the terms V potential energy functionals of the electron density ρ. Their subscripts specify whether terms apply to nuclear or electronic energy. This total energy functional may be rewritten in terms of orbitals χ_i as

$$E[\rho(\vec{\boldsymbol{r}})] = \sum_i^N \left(\left\langle \chi_i \middle| -\frac{1}{2}\vec{\nabla}_i^2 \middle| \chi_i \right\rangle - \left\langle \chi_i \middle| \sum_k^{nuclei} \frac{Z_k}{|\vec{\boldsymbol{r}}_i - \vec{\boldsymbol{r}}_k|} \middle| \chi_i \right\rangle \right) + \sum_i^N \left\langle \chi_i \middle| \frac{1}{2} \int \frac{\rho(\vec{\boldsymbol{r}}')}{|\vec{\boldsymbol{r}}_i - \vec{\boldsymbol{r}}'|} d\vec{\boldsymbol{r}}' \middle| \chi_i \right\rangle + E_{XC}[\rho(\vec{\boldsymbol{r}})] \quad \textbf{(4)}$$

where indices i and k run over the N electrons and the number of atoms, respectively; Z_k denotes the nuclear charge of atom k. The electron density ρ is, as common for Slater-determinantal wave functions, defined as

$$\rho = \sum_{i=1}^{N} \langle \chi_i | \chi_i \rangle \quad \textbf{(5)}$$

The orbitals χ_i needed to minimize E are found to satisfy the Schrödinger-like equations

$$\hat{h}_i^{KS} \chi_i = \varepsilon_i \chi_i \quad \textbf{(6)}$$

where ε_i are the orbital energies, and the one-electron KS operator is

$$\hat{h}_i^{KS} = -\frac{1}{2}\vec{\nabla}_i^2 - \sum_k^{nuclei} \frac{Z_k}{|\vec{\boldsymbol{r}}_i - \vec{\boldsymbol{r}}_k|} + \int \frac{\rho(\vec{\boldsymbol{r}}')}{|\vec{\boldsymbol{r}}_i - \vec{\boldsymbol{r}}'|} d\vec{\boldsymbol{r}}' + V_{XC} \quad \textbf{(7)}$$

most terms of which were already defined in Eq. 4, while the last term is the exchange-correlation potential

$$V_{XC} = \frac{\delta E_{XC}[\rho(\vec{\boldsymbol{r}})]}{\delta \rho(\vec{\boldsymbol{r}})} \quad \textbf{(8)}$$

The expression for the exchange-correlation energy that is characteristic to the B3LYP method [19, pp. 266-68] is

$$E_{XC}^{B3LYP} = (1-a)E_X^{LSDA} + aE_X^{HF} + bE_X^B + (1-c)E_C^{LSDA} + cE_C^{LYP} \quad \textbf{(9)}$$

the parameters of which expression were optimized to $a = 0.20$, $b = 0.72$ and $c = 0.81$. The superscript abbreviations refer to the *Local Spin Density Approximation*, Hartree-Fock, Becke [21] and Lee-Yang-Parr [22] functionals respectively [19].

When the molecular energy is minimized at E_0, the geometrical configuration is fixed. Based upon this geometry, its molecular vibrations and thermodynamic properties can be calculated. [23]. This computation requires the creation of a mass-weighed Hessian matrix out of the Cartesian Hessian:

$$f_{MWC\,i,j} = \frac{f_{Cart\,i,j}\Big|_{eq}}{\sqrt{m_i m_j}} = \left.\frac{\partial^2 V}{\partial q_1 \partial q_2}\right|_{eq} \quad \textbf{(10)}$$

where the m_i are the masses of the atoms in the molecule, and the compound displacement variables q_n thus become $q_1 = \Delta x_1\sqrt{m_1}$, $q_2 = \Delta y_1\sqrt{m_1}$, $q_4 = \Delta x_2\sqrt{m_2}$, and so on, covering the three spatial degrees of freedom of all atoms in the molecule. The subscript eq means at $E = E_0$.
A copy of this mass-weighed Hessian is diagonalized, yielding eigenvalues and eigenvectors of $3N$ normal modes – N now referring to the number of atoms. To sort these normal modes out, the origin of the coordinate system is shifted to the center of mass, and the inertia tensor $\boldsymbol{I}$ can be calculated:

$$\boldsymbol{I} = \begin{pmatrix} I_{xx} & I_{xy} & I_{xz} \\ I_{yx} & I_{yy} & I_{yz} \\ I_{zx} & I_{zy} & I_{zz} \end{pmatrix} = \begin{pmatrix} \sum_a m_a(y_a^2+z_a^2) & -\sum_a m_a(x_a y_a) & -\sum_a m_a(x_a z_a) \\ -\sum_a m_a(y_a x_a) & \sum_a m_a(x_a^2+z_a^2) & -\sum_a m_a(y_a z_a) \\ -\sum_a m_a(z_a x_a) & -\sum_a m_a(z_a y_a) & \sum_a m_a(x_a^2+y_a^2) \end{pmatrix} \quad \textbf{(11)}$$

(where index a refers to each individual atom) which, after being diagonalized, gives its eigenvalues and eigenvectors. The eigenvalues $\boldsymbol{I}'$ are the molecule's principal moments of inertia, and the matrix filled with the normalized eigenvectors, called $\boldsymbol{X}$, is needed for the extraction of the rotational modes form the $3N$ normal modes.

Next, the transformation matrix $\boldsymbol{D}$ is made as follows. Its three vectors are translational, with atomic indices $\sqrt{m_i}$ for the (x,y,z) element of atom i. The rotational vectors are defined as

$$\begin{aligned} D_{4\,j,i} &= \left((P_y)_i X_{j,3} - (P_z)_i X_{j,2}\right)/\sqrt{m_i} \\ D_{5\,j,i} &= \left((P_z)_i X_{j,1} - (P_x)_i X_{j,3}\right)/\sqrt{m_i} \\ D_{6\,j,i} &= \left((P_x)_i X_{j,2} - (P_y)_i X_{j,1}\right)/\sqrt{m_i} \end{aligned} \quad \textbf{(12)}$$

where i is the atomic index, j runs over (x,y,z), and P is the dot product of $\boldsymbol{R}$ (atomic coordinates with respect to the center of mass) and the corresponding row of aforementioned matrix $\boldsymbol{X}$. These six vectors are then normalized and checked for being normal modes. The number of translational and rotational modes is checked to correspond with the expected values: 3 for atoms, 5 for linear molecules, 6 otherwise. Schmidt orthogonalization generates the remaining vibrational mode vectors.

The produced matrix $\boldsymbol{D}$ then is used to transform the mass-weighed Hessian from Eq. 10 to internal coordinates, which is done as follows:

$$f_{Int.} = \boldsymbol{D}^{\dagger} f_{MWC} \boldsymbol{D} \tag{13}$$

From this Hessian in internal coordinates, the N_{vib}×N_{vib} submatrix, no longer containing the translational and rotational modes, is extracted and diagonalized, so that it gives N_{vib} eigenvectors and eigenvalues: the wavelengths λ_i. These wavelengths are converted to wavenumbers

$$\tilde{\nu}_i = \sqrt{\frac{\lambda_i}{4\pi^2 c^2}} \tag{14}$$

the units of which are finally all converted from atomic to more common macroscopic units. More properties for all these vibrations, such as reduced masses and displacements in Cartesian coordinates, are obtained, but not used in this work [23].

3.2. Statistical Mechanics

Statistical mechanics calculations rely on the definition of the partition function $q(V,T)$. This function is the statistical sum of all the possible states of the system, from which the values for the molar thermodynamic state functions at any given temperature can be derived. The standard molar entropy S, the enthalpy difference $(H(T) - H^0)$ and isobaric heat capacity C_P are calculated as

$$\begin{aligned} S(T) &= R \ln \frac{q}{N} + RT \left(\frac{\partial \ln q}{\partial T}\right)_P \\ H(T) - H^0 &= RT^2 \left(\frac{\partial \ln q}{\partial T}\right)_P \\ C_P(T) = \left(\frac{\partial (H(T) - H^0)}{\partial T}\right)_P &= 2RT \left(\frac{\partial \ln q}{\partial T}\right)_P + RT^2 \left(\frac{\partial^2 \ln q}{\partial T^2}\right)_P \end{aligned} \tag{15}$$

Under certain assumptions pointed out below, the partition function can be divided into four components: translational, rotational, vibrational and electronic motion, and the eventual system values of $S(T)$, $(H(T) - H^0)$ and $C_P(T)$ are the sum of its four contributions. These partition function components are now reviewed [24]. The first component is exemplary worked out below, application of the formulae in Eq. 15 to the other three, is included in Appendix A. The relation between the isochoric and isobaric heat capacities C_V and C_P is elaborated on in Appendix B.

The partition function of translational motion is defined as

$$q_t = \left(\frac{2\pi M k_B T}{N h^2}\right)^{3/2} \frac{V}{N} \tag{16}$$

where M is the molecular mass, k_B the Boltzmann constant, N the number of molecules, and h the Planck constant. The molecular volume V is approximated by the ideal gas law, thus $V/N = k_B T/P$. The partial differential of the partition function logarithm with respect to T is $5/(2T)$. So, the translational contributions to the molecular thermodynamics are

$$\begin{aligned} S_t(T) &= R \left(\ln \left(\left(\frac{2\pi M k_B T}{N h^2}\right)^{3/2} \frac{k_B T}{P} \right) + T \left(\frac{5}{2T}\right) \right) = R(\ln \frac{q_t}{N} + \frac{5}{2}) \\ (H(T) - H^0)_t &= RT^2 \left(\frac{5}{2T}\right) = \frac{5}{2} RT \\ C_{P_t}(T) &= \tfrac{5}{2} R \end{aligned} \tag{17}$$

At rotational motion, molecular geometry enters the stage. For single atoms, the partition function is just $q_r = 1$ and thus contributes nothing to the thermodynamic properties as both the logarithm and partial temperature derivative of 1 are zero. For linear molecules, like all diatomic ones, the partition function is

$$q_r = \frac{1}{\sigma}\left(\frac{T}{\Theta_r}\right) \tag{18}$$

where σ is the rotational symmetry number of the molecule, which is associated with the molecular symmetry point group, and with the rotational temperature $\Theta_r = h^2/(8\pi^2 I k_B)$, I being the moment of inertia. For general polyatomic molecules, the partition function looks a little more complicated:

$$q_r = \frac{\sqrt{\pi}}{\sigma}\left(\frac{T^{3/2}}{\sqrt{\Theta_{r,x}\Theta_{r,y}\Theta_{r,z}}}\right) \tag{19}$$

but it has essentially the same form as the translational partition function, $q \propto T^{3/2}$; all other parameters are molecular constants. For computational ease, the molecules are assumed to behave like rigid rotors.

The partition function of vibrational motion is more complex in nature than its translational and rotational counterparts, because its multiplicity is defined not by the three-dimensionality of space, but by the number N of atoms in the molecule, as $3N-6$ (or $3N-5$ in case of a linear molecule). The thermodynamic contributions from vibration are therefore the contributions of all individual modes K at frequencies ν_K with characteristic vibrational temperatures $\Theta_{v,K} = h\nu_K/k_B$ together. An additional complication is that either the potential well bottom or the first vibrational level (V=0) may be taken as reference. The difference between these two methods is the zero-point vibrational energy. Taking the well bottom as starting point, we are to consider the partition functions

$$q_{v,K} = \frac{e^{-\Theta_{v,K}/2T}}{1-e^{-\Theta_{v,K}/T}} \tag{20}$$

from which the overall partition function is calculated as the product of all these partition functions of the vibrations K. All molecular vibrations are assumed to be harmonic oscillations.

The electronic partition function can be written as

$$q_e = \sum_n \omega_n e^{-\epsilon_n/k_B T} \tag{21}$$

where ω_n is the multiplicity and ϵ_n the energetic level of electronic state n.
Here, the simplest approach assumes that all excited states ($n > 0$) are unavailable at all temperatures, which simplification is valid only for very low T. If then the electronic ground state ϵ_0 is put to zero, the partition function is curtailed to $q_e = \omega_0$, which is the spin multiplicity of the ground state [24]. This reduces the entropy contribution to $S_e = R\ln\omega_0$ and the energy and heat capacity contributions then are identically 0 [24]. In order to extend the validity of the calculated functions for higher temperatures, atomic energy levels are included in the calculation of the electronic contributions; the number of them that was considered, depends on the temperature.

Except the electronic ground state multiplicity, which is an input variable, all parameters in the process, which are the rotational symmetry number σ, the three-dimensional product of rotational constants (manually converted to moments of inertia) and vibrational frequencies, are printed in the DFT output files. Also, the zero-point energy E_{ZPE} and the sum of all aforementioned contributions to the energy, called total internal energy correction E_{tot} are explicitly given. Of the other listed values, only $H_{corr} = E_{tot} + k_B T$ is used for the calculation of formation enthalpies [24].

3.3. Phase Stability

Once the thermodynamic behavior of all molecules is known, the equilibrium composition of the system can be calculated. As all values calculated so far are only valid for the gas phase, data on the solid and liquid phases is either found in literature or approximated to complete the data set of the system.

For each compound, the stability of a phase at any given temperature T is given by the Gibbs free energy $G(T)$, which, in terms of the derived quantities, is defined [25] as

$$G(T) = \Delta H_f^0(298\ K) - TS^0(298\ K) + \int_{298}^{T} C_p(T)\ dT - T\int_{298}^{T}\left(\frac{C_p(T)}{T}\right) dT \qquad \textbf{(22)}$$

where, as elsewhere, ΔH_f^0 is the formation enthalpy of the compound at 298 K, S^0 the standard entropy at that same temperature, and $C_P(T)$ the isobaric molar heat capacity, for that phase.

When all these values for all possible phases are calculated, the next step is to find the energetically lowest phase composition given the elemental composition and the temperature of the system. A phase diagram is the common graphical way to depict the most stable status of the system. Its axes run over the system parameters, which are the elemental composition and the temperature. Each tile in the diagram stands for the combination of compounds that is most stable within the temperature and composition boundaries of the tile. Crossing a line from one tile to another, therefore, means a phase transition or a shift in reaction equilibrium.

Another important variable is the fluorine potential (Eq. 2). The phase diagram showing the relations between the temperature and the fluorine potential of the system is called an Ellingham diagram. The data in this diagram are important to the fluorine potential management.

A third diagram shows the composition of the system of ruthenium and fluorine as a function of the elemental composition. In case of a stable gas phase, it predicts what amounts of what compounds will be found in the off-gas flow; for condensed phases, it indicates what compounds are present in the reactor core. The physical state of the present compounds then need to be evaluated to predict whether they are most likely to be dissolved in the salt mixture or settled on the reactor surfaces.

These calculations are done by a program, called *FactSage*, that implements the CALPHAD methodology [26]. The term CALPHAD is acronymic for *CALculation of PHAse Diagrams*, which states exactly what it does. The main strengths of this approach are that subsystems can be combined to describe a larger, multi-component system, and that it allows refinement of its input parameters to improve the correspondence between the calculations and experimental data. Because of the former quality, it is not yet necessary to take into account the complete set of other MSR contents, such as lithium, beryllium, uranium, and all its decay products. The latter attribute is very helpful for (sub)systems constituted of poorly examined components like the ruthenium fluorides.

4. Experimental

4.1. Geometrical Calculations

Calculation of molecular structures using DFT was done by the *Gaussian* program [27] using the B3LYP method. The quasi-relativistic ECP28MWB pseudopotentials and corresponding basis set used on the ruthenium atoms were taken from the University of Cologne [28], where its Department of Theoretical Chemistry keeps a database of energy-consistent pseudopotentials as correct as possible. On the fluorine atoms, the in-program cc-pVTZ basis set was used. The calculation route

$$\text{\# B3LYP/gen pseudo=read opt freq pop=none} \quad \textbf{(23)}$$

was taken for all possible multiplicity states in all attempted starting geometries of the investigated molecules. The keyword opt commands optimization of the molecular geometry in the input file, and freq prompts calculation of the molecular vibrational frequencies and derived thermochemical properties. These operations are carried out as described above.
Multiplicity of the electronic state is conform its definition calculated as $2S + 1$, S being the total spin angular momentum. This can be simplified by the consideration that paired electrons, including all the core electrons, cancel out each other in this calculation; hence, the product $2S$ in all cases simply reduces to the number of unpaired valence electrons. Initial parameter guesses are listed in Table 2. The one multiplicity number that yielded the most stable molecular geometry is retained and used through the following calculations.

Once the multiplicity of the electronic ground state, molecular geometry and corresponding symmetry point group were confirmed, tight conversion via the route

$$\text{\# B3LYP/gen pseudo=read opt=tight int=ultrafine scf=conver=9 freq pop=none} \quad \textbf{(24)}$$

was applied to that molecule to compute the structural and thermodynamic parameters more accurately. In any doubt on the exact structure, tight conversion was applied to all configurations in question, after which the most stable conformation was kept.

Since the pentafluoride trimer configurations (C_{3v} and C_S) differed very little energetically, both conformations were retained. Additionally, they were checked and confirmed to have reached the true ground state within their respective symmetries by a special *Gaussian* operation taking as input the optimized geometry from the check file made during the calculation. The command for this computational route is

$$\text{\# B3LYP/gen pseudo=read geom=check guess=read Stable=Opt pop=none} \quad \textbf{(25)}$$

Table 2: Initial guesses for geometries (point groups), ground state multiplicities and bond lengths for the DFT calculations. Most bond lengths were taken from literature, see Table 1.

	RuF	**RuF_2**	**RuF_3**	**RuF_4**	**RuF_5**	**RuF_6**	**$(RuF_5)_2$**	**$(RuF_5)_3$**
PGs	$C_{\infty v}$	$D_{\infty h}$, C_{2v}	D_{3h}, C_{3v}, C_{2v}	D_{4h}, T_d, C_{3v}, C_{2v}	D_{3h}, C_{4v}, D_{5h}	O_h	D_{2h}	C_{3v}, C_S, D_{3h}
GS mult.	2, 4, 6, 8	1, 3, 5, 7	2, 4, 6	1, 3, 5	2, 4	1, 3	1, 3, 5, 7	2, 4, 6, 8, 10
Bonds (Å)	2.05	1.96	1.9	1.87	1.87	1.8775	2.0 (b), 1.85 (ax), 1.77 (eq)	

During the calculations, some expected symmetries broke down to lower levels. In these cases, the newly obtained symmetries were then used as input to be optimized, going through the complete DFT process again, with the most recently obtained bond lengths and all possible ground state multiplicities.

In addition to the compounds, the ruthenium and fluorine atoms were calculated through, because the output on these elements is a reference state for the enthalpy calculations.

4.2. Thermodynamic Calculations

From the energetic DFT output data mentioned above on all molecules and both elements, values for the standard enthalpy of formation $\Delta H_f^{298\,K}$ were calculated as follows [24]:

$$\Delta H_{f(compound)}^{298\,K} = \Delta H_{f(compound)}^{0\,K} + \Delta H_{(compound)}^{298\,K-0\,K} - \sum \Delta H_{(atoms)}^{298\,K-0\,K} \quad \textbf{(26)}$$

$$\Delta H_{f(compound)}^{0\,K} = \sum \Delta H_{f(atoms)}^{0\,K} - \Delta E_{atomization} \quad \textbf{(27)}$$

$$\Delta H_{(compound)}^{298\,K-0\,K} = (H_{corr} - E_{ZPE})_{compound} \quad \textbf{(28)}$$

$$\Delta E_{atomization} = \sum (E_0 + E_{ZPE})_{atoms} - (E_0 + E_{ZPE})_{compound} \quad \textbf{(29)}$$

For the fluorine atom, $\Delta H_{(F)}^{298\,K-0\,K}$ was taken as half of the value for elemental fluorine (F_2). Reference values for $\Delta H_{(atoms)}^{298\,K-0\,K}$ and $\Delta H_{f(atoms)}^{0\,K}$ were taken from JANAF tables [29] for fluorine and from the NBS tables [30] for ruthenium.

Gaussian does some thermodynamic analysis on the molecule, but it neglects the electronic contributions to the thermodynamics [24]; therefore, entropy and the heat capacity calculations were done by a program called *MoTher*, short for *Molecular Thermodynamics*. Because the electronic energy levels up to 30000 cm^{-1}, as obtained from Moore [31], are put in, *MoTher* is able to also calculate the electronic contributions to the entropy and heat capacity. Only a limited range of energy levels is put in to save time, as a result of which the value ranges for the heat capacity $C_P(T)$ and molar entropy $S(T)$ are valid only on a temperature range of 298-3000 K. As the MSR temperature normally is around 900 K, this range is large enough to regard the results meaningful to the reactor operation. From the entropy, only the value at 298 K is needed. To the heat capacity values, a function was fitted, having the general formula

$$C_P(T) = A + BT + CT^2 + D/T^2 + ET^3 + F/T \quad \textbf{(30)}$$

with F only non-zero when a reasonable fit could not be obtained with $F = 0$. The fit is accepted reasonable when $R^2 > 0.999$.

4.3. Phase Diagram Calculations

The calculated gas-phase data have to be complemented with thermodynamic data on the liquid and solid phases of the compounds. As little information is available in literature, most of these are to be estimated. The values and functions for the entropy and heat capacity of the RuF_3, RuF_4 and RuF_6 solids were obtained from the Neumann-Koop rule:

$$f(\mathrm{RuF}_n, \mathrm{s}) = \tfrac{1}{5}(n \times f(\mathrm{RuF}_5, \mathrm{s}) + (5 - n) \times f(\mathrm{Ru}, \mathrm{s})) \quad \textbf{(31)}$$

with f either the entropy S^0 or heat capacity $C_P(T)$ function. The form of this rule is based on the equilibrium reaction

$$n\ \mathrm{RuF_5\ (s)} + \mathrm{Ru\ (s)} \leftrightarrow 5\ \mathrm{RuF}_n\mathrm{(s)} \quad \textbf{(32)}$$

Then, some post-calculation CALPHAD optimizations had to be done also on the formation enthalpy of some of the gaseous molecules, particularly on the higher ruthenium fluorides. The combination of the calculated and otherwise generated data did not accurately reproduce the thermodynamic properties of these molecules, such as melting point, boiling point, and decomposition temperatures. The calculated formation enthalpies were therefore optimized to fit the experimental data.

The phase, Ellingham and equilibrium diagrams were computed by the *FactSage* modules *Phase Diagram* and *Equilib*, based on calculated, optimized and additionally looked up parameters.

5. Results and Discussion

5.1. Molecular Geometry

The DFT-calculated structures of the ruthenium fluoride compounds are shown in Figure 1; the computed parameter values of these molecules are included in Table 3.

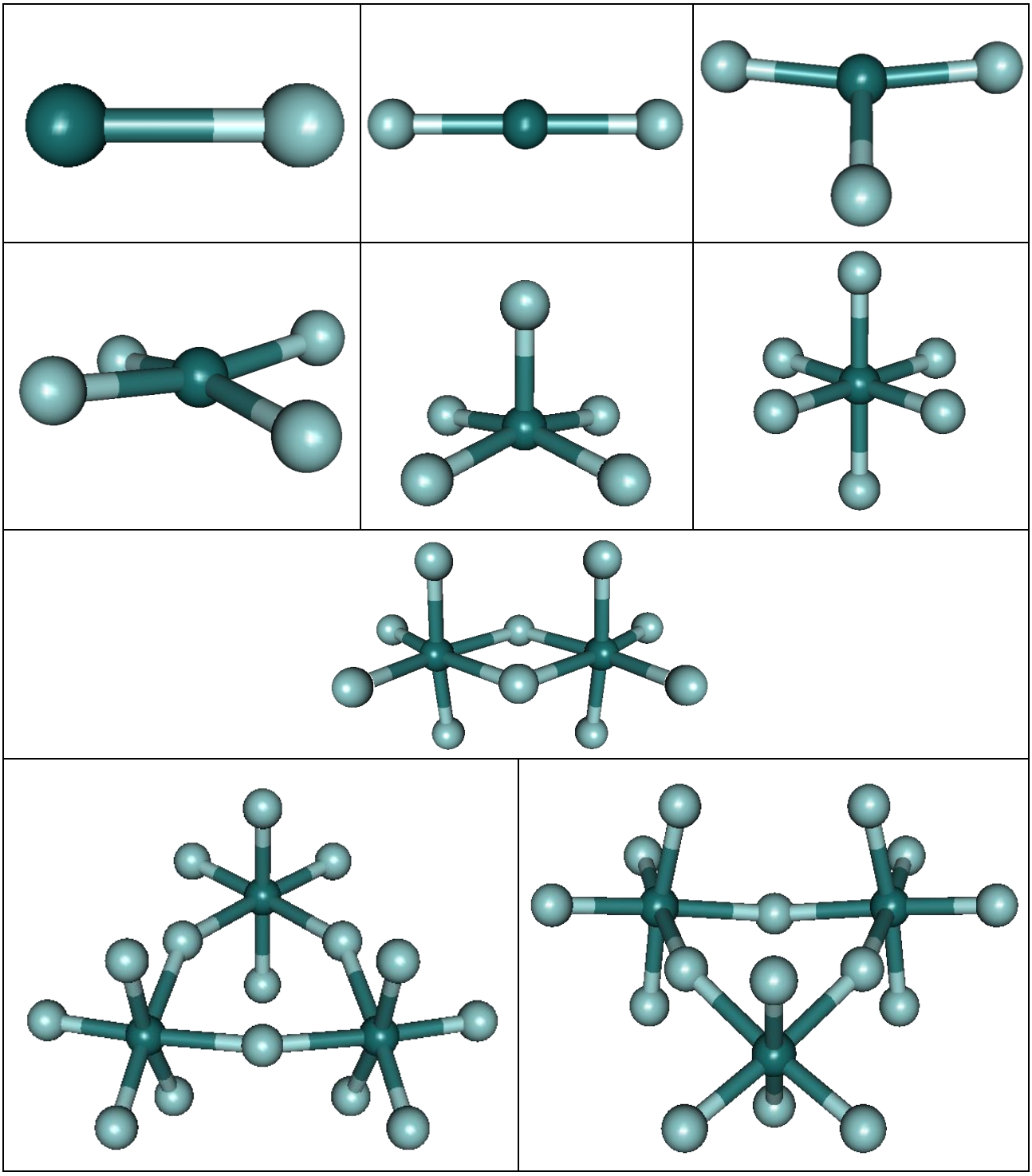

Figure 1: Ball-and-stick models of the ruthenium fluorides; ruthenium in darker grey, fluorine in lighter grey. Left to right: mono-, di- and trifluoride; tetra-, penta- and hexafluoride; pentafluoride dimer; pentafluoride trimers in chair, boat conformation.

Table 3: Calculated molecular parameters of the gaseous ruthenium fluorides, as well as the elemental data needed for the thermodynamic calculations.

Species	Point Gr.	GS mult.	Bond lengths Å	Bond angles °	Rotational constants GHz	Vibrational frequencies cm^{-1}	Moments of inertia $I_X \cdot I_Y \cdot I_Z$ $(kg \cdot cm^2)^3$
Ru		5					
F		2					
RuF	$C_{\infty v}$	4	1.8943		8.79493	599.33	*9.5420E-46* [n1]
RuF_2	$D_{\infty h}$	5	1.8734	180	3.78977	141.48 (2), 609.51, 680.42	2.2144E-45 [n2]
RuF_3	C_s	4	1.8503, 1.8499 (2)	99.7 (2), 160.3	7.72588 4.00158 2.63839	139.77, 142.38, 171.71, 517.07, 650.75, 694.52	7.2460E-135
RuF_4	D_{2d}	5	1.8453	168.7 (2)	3.86837 (2) 1.97205	48.95, 179.38, 249.11 (2), 269.20, 621.59, 676.59, 717.65	2.003E-134
RuF_5	C_{4v}	4	1.797 (ax), 1.837 (eq)	97.8 (ax-eq)	2.64824 (2) 2.00726	120.73, 166.99 (2), 237.52, 266.11 (2), 273.85, 631.49, 684.61, 720.60 (2), 734.38	4.1986E-134
RuF_6	D_{4h}	3	1.832 (ax) 1.806 (eq)	90	2.02884 1.99621 (2)	156.76 (2), 214.28, 276.85 (2), 322.59, 327.68, 390.13 (2), 629.69, 635.97, 702.43, 731.67, 744.60 (2)	7.3107E-134
$(RuF_5)_2$	D_{2h}	7	1.832 (ax), 1.806 (eq), 2.0324 (b)	91.998 (ax-eq), 87.649 (ax-b), 95.560 (eq-eq), 94.492 (eq-b), 75.457 (b-b)	1.12520 0.33691 0.32401	65.82, 90.66, 107.74, 133.49, 144.13, 153.32, 200.84, 206.85, 243.28, 234.76, 241.53, 242.41, 259.56, 260.95, 266.87, 270.75, 297.22, 304.38, 368.57, 445.41, 460.52, 486.95, 662.48, 663.06, 713.43, 721.92, 724.44, 732.07, 742.01, 746.44	4.8119E-132
$(RuF_5)_3$	C_{3v}	10	1.832 (ax), 1.804 (eq), 2.017 (b)	86.80 (ax-b), 94.25 (eq-eq), 86.75 (b-b)	0.22397 (2) 0.13458	27.18 (2), 40.16, 95.40 (2), 98.19, 113.48 (2), 138.55 (2), 145.48, 147.79, 200.28 (2), 211.96, 215.63 (2), 234.13 (2), 239.11, 243.17, 256.67, 262.53 (2), 271.54 (2), 273.04, 275.17 (2), 297.72, 328.78, 332.62, 332.62, 462.49, 543.03 (2), 663.03, 665.66 (2), 711.66, 724.79 (2), 726.13 (2), 733.98 (2), 744.68, 748.91	8.7550E-131
$(RuF_5)_3$	C_s	10	1.83 (ax), 1.80 (eq), 2.02 (b)	86.84 (ax-b), 94.32 (eq-eq), 86.74 (b-b)	0.22727 0.22436 0.13578	20.80, 28.42, 38.98, 87.25, 93.41, 103.65, 112.57, 118.15, 131.26, 136.41, 145.28, 151.54, 203.70, 204.11, 208.54, 214.26, 216.72, 230.13, 233.26, 238.58, 242.22, 254.94, 261.72, 263.40, 268.64, 270.67, 271.03, 276.03, 285.67, 296.49, 328.16, 339.86, 343.49, 460.97, 539.11, 540.39, 662.86, 665.32, 665.41, 711.23, 722.94, 723.41, 726.59, 727.17, 733.31, 744.08, 748.37	8.5266E-131

n1: Only a one-dimensional number (i.e. unit is **$kg \cdot m^2$**) because the molecule is linear. Calculated but not used as a diatomic molecule requires a different way of input in *MoTher*.
n2: Only a one-dimensional number (i.e. unit is **$kg \cdot m^2$**) because the molecule is linear.

The geometry of the two lowest ruthenium fluorides nicely corresponds with the literature values [11], [14], [15]; only the bond lengths here are shorter. The same holds for RuF_5 [11], [12], [16].

As said, some molecules were calculated to have a lower level of symmetry than initially expected. On RuF_3, C_{3v} became C_S; RuF_6 reduced its symmetry to D_{4h}; on RuF_4, T_d broke down to a totally disordered C_S, the structure of which was visually recognized as an attempt to get D_{2d} – which was not reached because *Gaussian* cannot recognize higher symmetries out of optimizing lower ones.

The irregular shape of the trifluoride is yet to be explained. If the molecule were flat, it would have C_{2v} symmetry; if all its F-Ru-F angles were equal, it would be C_{3v}. The remarkable result, having only C_S symmetry, is halfway between the options with higher symmetry.

The symmetry point group of ruthenium hexafluoride (D_{4h}) also appeared not to be the expected O_h. However, Jahn-Teller distortions, already expected when the molecule was first investigated [8], were observed by spectroscopic studies [11], [32], which indicates that its molecular symmetry is indeed not perfectly octahedral. As reported in Table 3, it suffers from axial elongation. Another recent study [17], using a slightly different calculation method, also found a similar, tetragonally distorted D_{4h} structure (although with shorter bonds) as ground state, and reports a small (2.5 kJ/mol) interconversion barrier to the perfect octahedral O_h geometry, which may well explain the weakness of the Jahn-Teller effect.

For the tetrafluoride, the D_{2d} molecule reported here is in good agreement with the molecular structure of niobium tetrafluoride [25]. Considering this structure and its relationship with the T_d and D_{4h} structures which have been reported [11], [12], [16], I expect a parabola-like course of the energy level, having the D_{2d} structure calculated here as minimum, and the flat and tetrahedron structures on either side of the atom displacement axis. This model correctly explains why the flat structure is more stable than the tetrahedron: because it is closer (in terms of atom displacement needed) to the calculated ground state geometry.

The structures of the di- and trimers of ruthenium pentafluoride show no unexpected measures, they nicely agree with the electron diffraction measurements reported in [10], [11].

5.2. Molecular Thermodynamics

The calculated values for the standard formation enthalpy and molar entropy from the DFT computations are listed in Table 4. The formation enthalpies neatly follow the same trend as the literature values. Nearly all values are close to those in [13]; however, for RuF the calculated formation enthalpy corresponds better with [9], and the four largest molecules (hexafluoride and pentafluoride dimer and trimers) are all calculated to be approximately 100 kJ/mol more stable than [13] calculated. Especially regarding the hexafluoride, described as highly reactive and known to decompose to ruthenium pentafluoride and elemental fluorine [8], this is quite remarkable, and possibly further away from reality than [13]'s values.
The molar entropy values, on the other hand, show the expected features: numbers increase generally with the amount of atoms in the molecule, while molecules of higher symmetry and/or with internal rings have reduced entropy as they have fewer degrees of freedom.

Table 4: Calculated values for formation enthalpy and molar entropy for the gas-phase ruthenium fluorides at 298.15* K *from DFT computations.

Species	ΔH_f^0 kJ/mol	S^0 J/(mol·K)
RuF	324.43	233.67
RuF_2	–126.09	261.21
RuF_3	–368.89	330.28
RuF_4	–640.96	344.23
RuF_5	–827.10	357.72
RuF_6	–932.37	355.19
$(RuF_5)_2$	–1808.3	515.39
$(RuF_5)_3$ C_{3v}	–2743.8	704.27
$(RuF_5)_3$ C_S	–2744.3	718.14

Parameter values for the calculated molar isobaric heat capacity Eq. 30 as computed by *MoTher* are given in Table 5.

Table 5: Parameters for Eq. 30 to fit the heat capacity function of the gaseous ruthenium fluorides.

Species	A	B	C	D	E	F
RuF	81.82795	–0.02306	5.25696E-6	3.22103E6	–2.25792E-10	–23102.42767
RuF_2	147.52073	–0.05968	1.79678E-5	4.70101E6	–1.99256E-9	–38777.87151
RuF_3	78.29614	0.0066	–3.08214E-6	–9.34619E5	4.74228E-10	0
RuF_4	99.49598	0.01167	–5.44031E-6	–1.49949E6	8.36277E-10	0
RuF_5	121.55812	0.01556	–7.25225E-6	–1.96018E6	1.11431E-9	0
RuF_6	143.35432	0.01984	–9.25174E-6	–2.72021E6	1.42190E-9	0
$(RuF_5)_2$	260.88445	0.0296	–1.38041E-5	–4.33956E6	2.12178E-9	0
$(RuF_5)_3$ C_{3v}	399.57647	0.04448	–2.07362E-5	–6.39571E6	3.18684E-9	0
$(RuF_5)_3$ C_S	399.63709	0.0444	–2.07002E-5	–6.39972E6	3.18143E-9	0

An overview of the individual contributions to the entropy and heat capacity at 298 K from all molecular motion are given in Table 6. The entropic contributions, as did their sums in Table 4, follow the expected trends: higher entropy with larger molecule for translation and rotation, slight deviations downwards for vibration on the molecules of higher symmetry. The translational and rotational contributions to the heat capacity clearly show the molecule's spatial dimensions of motion, and the vibrational contribution logically increases with the number of possible modes. The electronic contributions are zero from RuF_3 onwards because no electronic levels are available for Ru(III) and higher [31].

***Table 6: Contributions to the entropy and heat capacity from translational, rotational, vibrational and electronic motion of the gaseous ruthenium fluorides at 298* K.**

Species	Entropy ($S^0(298)$) J/(mol·K)				Heat Capacity ($C_P(298)$) J/(mol·K)			
	Transl.	**Rot.**	**Vib.**	**El.**	**Transl.**	**Rot.**	**Vib.**	**El.**
RuF	168.572	2.198	62.859	0.045	20.786	8.315	4.684	0.296
RuF_2	170.404	26.488	64.096	0.218	20.786	8.315	23.859	1.082
RuF_3	172.001	38.888	107.865	11.526	20.786	12.472	36.318	0
RuF_4	173.416	56.870	100.566	13.382	20.786	12.472	52.538	0
RuF_5	174.687	67.865	103.643	11.526	20.786	12.472	70.475	0
RuF_6	175.841	70.032	100.185	9.134	20.786	12.472	84.884	0
$(RuF_5)_2$	183.332	192.525	123.354	16.179	20.786	12.472	186.847	0
$(RuF_5)_3$ C_{3v}	188.389	361.318	135.415	19.145	20.786	12.472	306.447	0
$(RuF_5)_3$ C_S	188.389	363.722	146.832	19.145	20.786	12.472	306.441	0

5.3. System Assessment

In Table 7, the *FactSage* input figures are listed that are not directly obtained from the calculations by and based on DFT, but that were found in literature, approximated, or optimized to fit experimental data.

The formation enthalpy of RuF_3 (s) was optimized using data from the Oak Ridge National Laboratory (ORNL) Molten Salt Reactor Experiment (MSRE) [3]. Interestingly, this value differs over 300 kJ/mol from the gas-phase value – a rather large number for a sublimation enthalpy. However, Nikitin and Zbezheva [13] calculated a similar value.
The solid RuF_4 formation enthalpy was optimized based on experimental data from Nikitin and Zbezheva [13]. The resulting number is also close to their reported value.
The RuF_6 formation enthalpies of all phases were optimized to fit the data on its vapor pressure and boiling point from [8].
The RuF_5 system has the most secure experimental background, as its solid phase enthalpy of formation was measured by bomb calorimetry [18]. The solid-phase entropy and heat capacity values, as well as data on the liquid phase was taken from [33]. The complex gas phase of the pentafluoride, which consists of monomeric, dimeric and trimeric molecules, had the formation enthalpies of its constituents optimized based on the total RuF_5 pressure as reported in [34]. Also, from this point onwards, only the most stable conformer of the RuF_5 trimer, in C_S symmetry, represented the trimer on its own. It is, however, safe to assume that both configurations of the pentafluoride trimer will be present in their known ratios [10].
The molar entropies and heat capacities for the solids, except for RuF_5, were obtained from the Neumann-Koop rule.

For RuF_6 and the pentafluoride oligomers, the optimized values for the formation enthalpy come closer to those that [13] calculated; the optimized RuF_5 monomer is significantly more stable than their calculations.

Table 7: FactSage input obtained by optimization calculations.

Species	ΔH_f^0 **(298 K) kJ/mol**	S^0 **(298 K) J/(mol·K)**	C_P **J/(mol·K)**
RuF_3 (s)	–690.444	108.06	81.17 + 0.05T
RuF_4 (s)	–838.09	134.57	101.2528 + 0.05021T
RuF_6 (s)	–937.50	187.59	140.72 + 0.0805T
RuF_6 (l)	*ΔH_{fus} = 4.50 kJ/mol at 327 K*		190
RuF_6 (g)	–829.019		
RuF_5 (s)	–892.866	161.084	124.55 + 0.0692T
RuF_5 (l)	*ΔH_{fus} = 18.828 kJ/mol at 359.65 K*		182.004
RuF_5 (g)	–802.253		
$(RuF_5)_2$ (g)	–1692.586		
$(RuF_5)_3$ (g)	–2577.863		

The resulting diagrams seem to be reasonable. The Ru-F_2 phase diagram, featured in Figure 2, shows the preferred oxidation states of ruthenium as they depend on the fluorine availability. The most prominent vertical phase boundaries are the lines at $\mathrm{F_2/(Ru + F_2)} = 0.6$, the exact ratio of RuF_3, at $\mathrm{F_2/(Ru + F_2)} = 0.\overline{667}$, equal to RuF_4, and at $\mathrm{F_2/(Ru + F_2)} \cong 0.714$, corresponding to RuF_5. The RuF_6 line at $\mathrm{F_2/(Ru + F_2)} = 0.75$ too is discernible. From the horizontal phase transitions, the melting points of both RuF_6 ($T = 327\ \mathrm{K}$) and RuF_5 ($T = 360\ \mathrm{K}$) as well as the RuF_5

boiling point around $T \sim 500\ \mathrm{K}$ are clearly visible. Also, the RuF_4 decomposition temperature at $T \sim 930\ \mathrm{K}$ is featured.

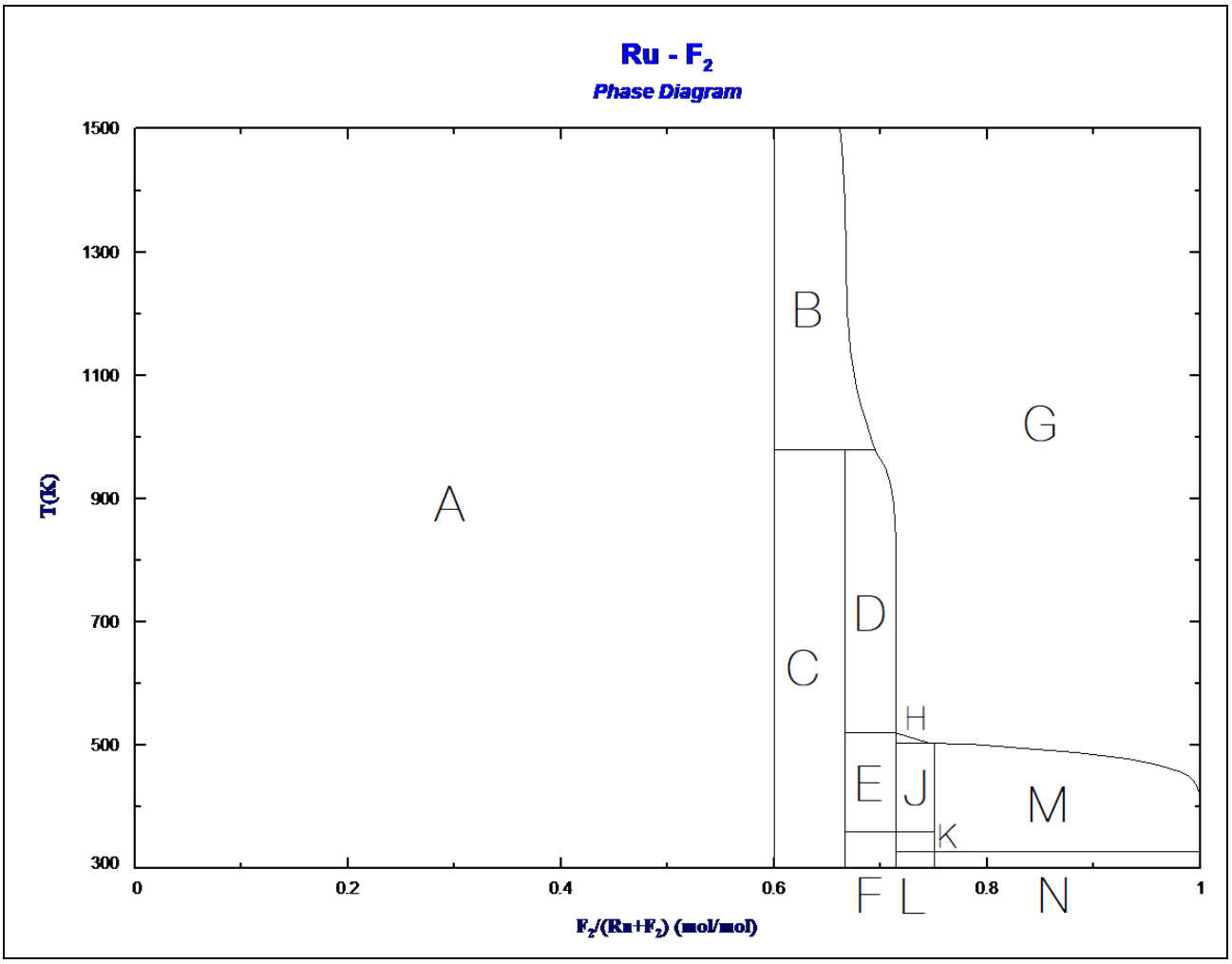

Figure 2: Calculated phase diagram of the Ru-F_2 system. Horizontal axis: mole fraction of molecular fluorine; vertical axis: temperature in* K. *Pressure: 1 atm.
Indicated phases:* A *Ru (s), RuF_3 (s);* B *RuF_3 (s), gas mixture;* C *RuF_3 (s), RuF_4 (s);* D *RuF_4 (s), gas mixture;* E *RuF_4 (s), RuF_5 (l);* F *RuF_4 (s), RuF_5 (s);* G *gas mixture;* H *RuF_5 (l), gas mixture;* J *RuF_5 (l), RuF_6 (l);* K *RuF_5 (s), RuF_6 (l);* L *RuF_5 (s), RuF_6 (s);* M *RuF_6 (l), gas mixture;* N *RuF_6 (s), gas mixture.
All gas mixtures are assumed to be ideal.

The Ellingham diagram is shown in Figure 3. Again, the tri- and tetrafluoride are the dominant compounds, and a significant part of the picture is taken by metallic ruthenium. Evaluating this diagram at 900 K, the standard MSR operation temperature, the following transition points are estimated: $\mathrm{Ru\ (s)} \leftrightarrow \mathrm{RuF_3(s)}$ at $\Delta\overline{G}_{F_2} \cong -320$ kJ/mol, $\mathrm{RuF_3\ (s)} \leftrightarrow \mathrm{RuF_4(s)}$ at $\Delta\overline{G}_{F_2} \cong -150$ kJ/mol, and $\mathrm{RuF_4\ (s)} \leftrightarrow \mathrm{(g)}$ at $\Delta\overline{G}_{F_2} \cong -120$ kJ/mol.

Assuming that the system properties are correctly described, ruthenium is under MSR conditions mainly present as metallic solid, as the typical fluorine potential is about $\Delta\overline{G}_{F_2} \cong -700$ kJ/mol.

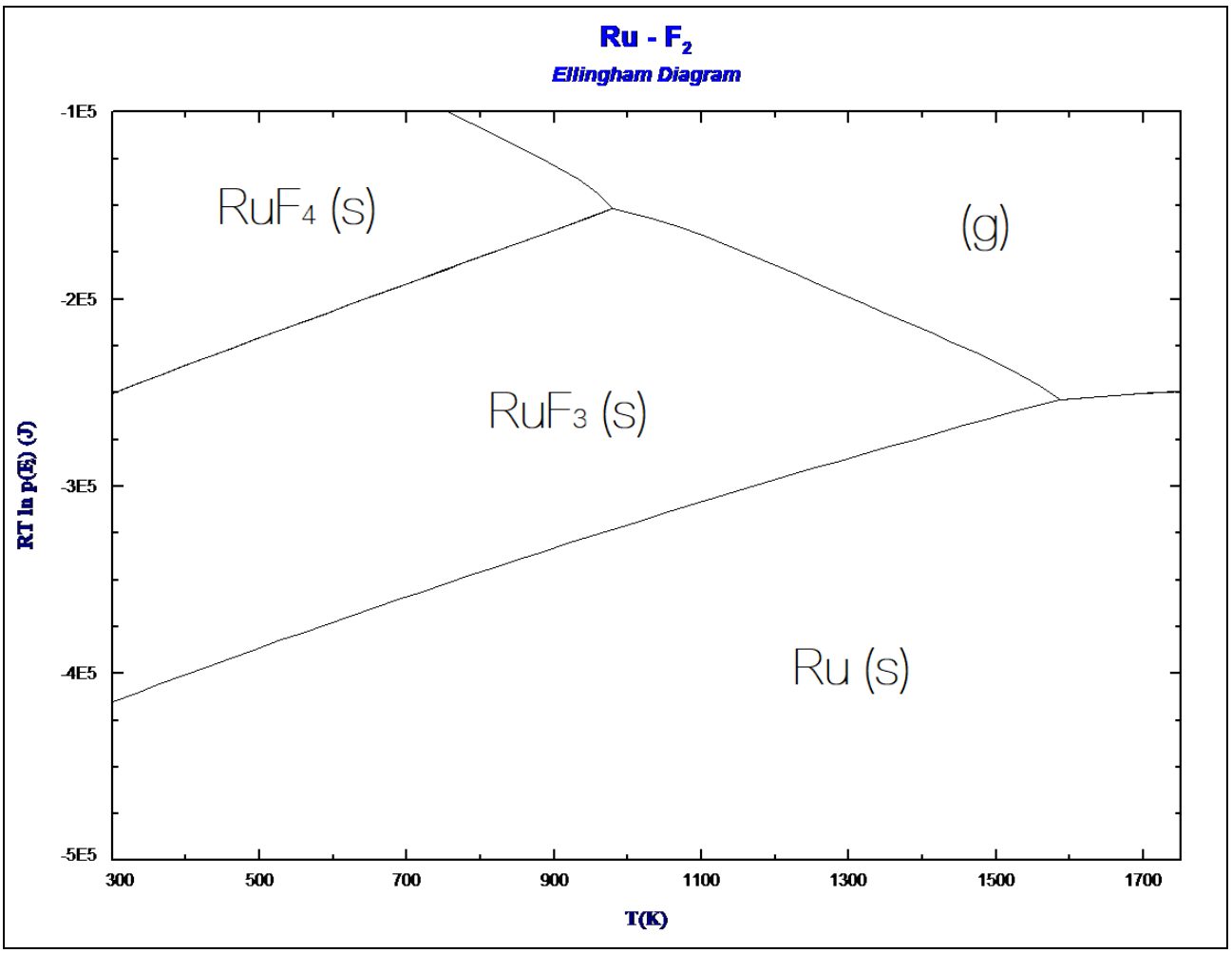

Figure 3: Calculated Ellingham diagram. Horizontal axis: temperature in* K*; vertical axis: fluorine potential in* J/mol*. The gas mixture* (g) *is assumed to be ideal.

Figure 4 shows the gas-phase composition cross-section at 900 K. Consistent with the two diagrams above, RuF_3 and RuF_4 dominate the picture when fluorine is limitedly available, and the higher fluorides are only there when enough fluorine is supplied; RuF is completely absent.

Figure 5 puts the calculations on ruthenium fluorides from this work into perspective. Compared to the niobium and molybdenum Ellingham diagrams, ruthenium is positioned at higher, less negative fluorine potentials. Thus, when the noble metal precipitate is to be separated by fluorination, increasing the fluorine pressure (thus the fluorine potential) will affect niobium first, then molybdenum, followed by ruthenium.
Transition metals in higher-numbered groups tend to become more noble, so the bottom-to-top order $_{41}$Nb – $_{42}$Mo – $_{44}$Ru neatly follows expectations. If needed, reasonable $_{43}$Tc data could be interpolated from this diagram.

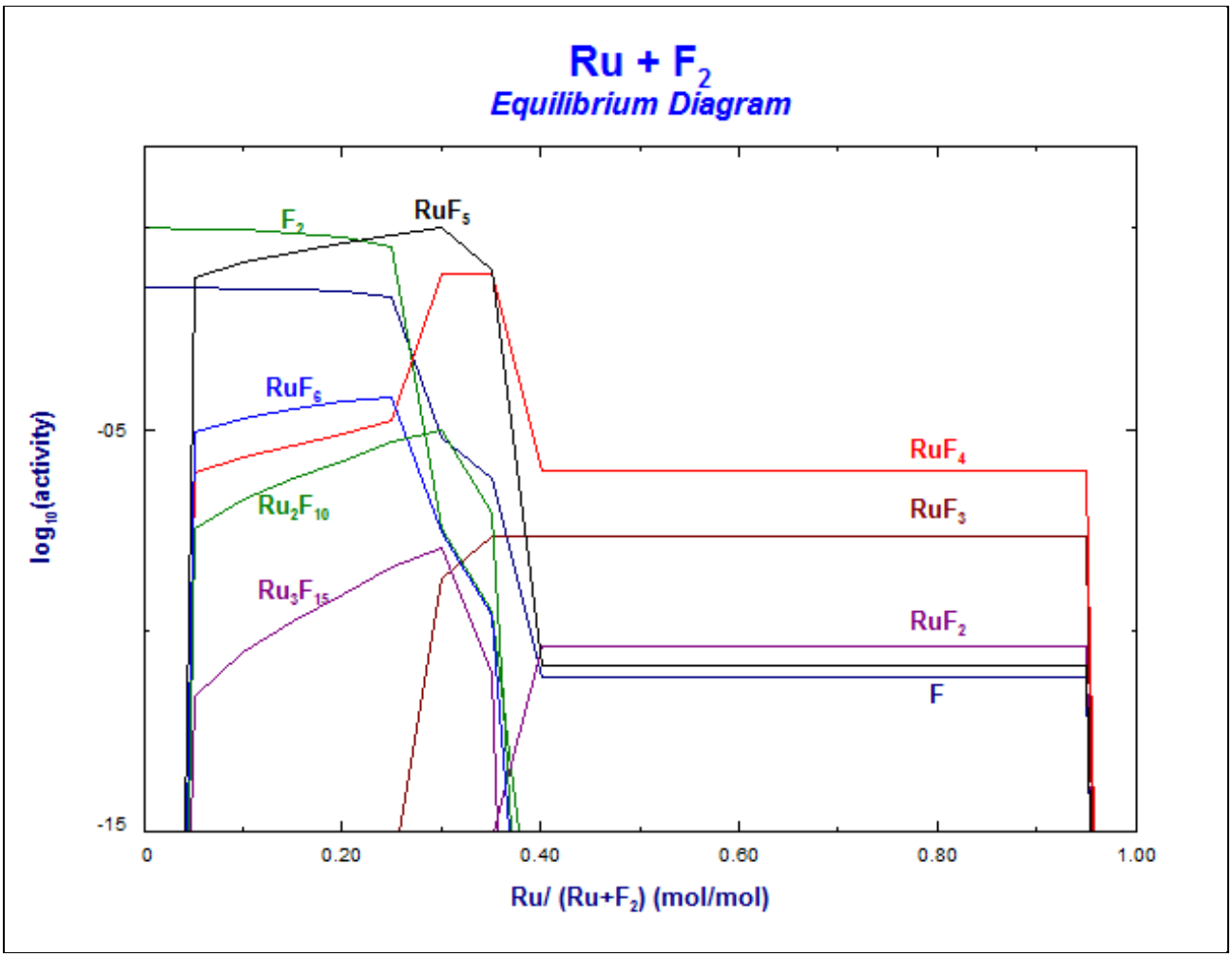

Figure 4: Calculated composition of the gas phase at 900* K *and atmospheric pressure. Horizontal axis: mole fraction of ruthenium; vertical axis: logarithm (base 10) of species activity, which equals partial pressure for ideal gases on the left-hand side of the graph.

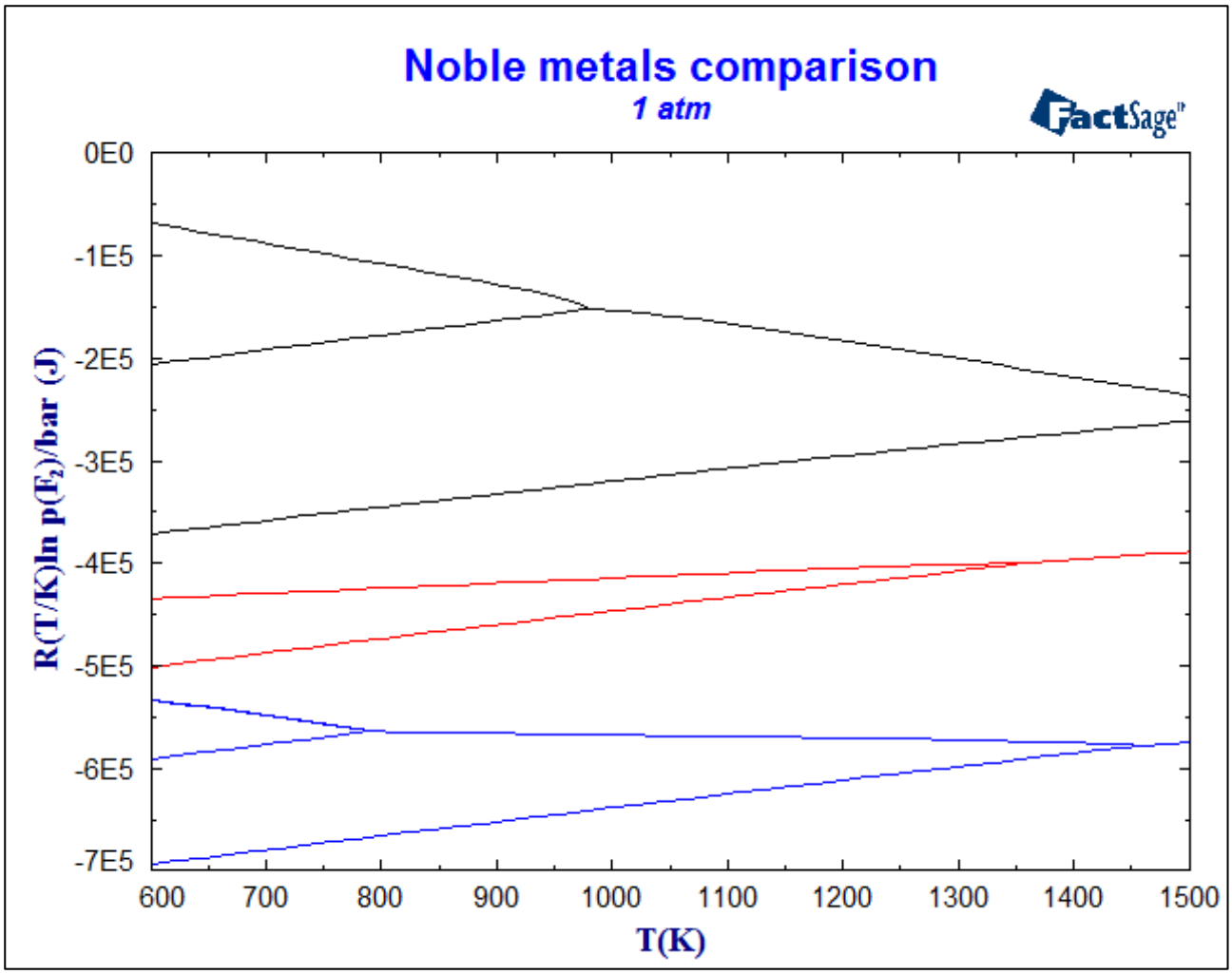

Figure 5: Ellingham diagram of $_{44}$Ru (black, see Fig. 3) and its neighbors $_{41}$Nb (blue)and $_{42}$Mo (red). Drawn using previously calculated data on the niobium* [25] *and molybdenum fluoride systems.

6. Conclusion

6.1. Conclusion

The thermochemical behavior of the Ru-F subsystem under MSR conditions has successfully been assessed by CALPHAD computations, mainly using data on the ruthenium fluoride compounds as generated by DFT/B3LYP and statistical mechanics calculations.
From the computed data, ruthenium appears to be the mostly present in its metallic solid state in a MSR-like environment at 900 K and atmospheric pressure. The amount of fluoride anions available per atom of ruthenium is expected to be limited, as the fuel salt contains only four per molecule. Hence, it seems reasonable that metallic ruthenium dominate the system.
The positioning of the ruthenium compounds in the Ellingham diagram is consistent with the placement of ruthenium in its row of transition metals, as it is just less easily fluorinated than its neighbor noble metals niobium [25] and molybdenum.

The general picture of the thermochemistry of ruthenium fluorides in a MSR environment is now made clear; to obtain more accurate results, needing less optimizations afterwards, and to thereby make more reliable predictions, a couple of issues yet has to be solved.

6.2. Recommendations

First and foremost, more experimental data on the thermodynamics of ruthenium fluorides is needed to either confirm or correct all individual numbers used here. The most important compounds for further research are RuF_3 and RuF_4, as they dominate the high-temperature chemistry of the system. The most important knowledge yet to be acquired is thermochemical and geometrical. Especially calorimetry, IR and Raman spectroscopy, and electron diffraction studies are desired.
Secondly, the ongoing progress of computational chemistry will be eager to use that generated data to produce and refine the molecular modeling at all levels. Ultimately, even less post-calculation optimizations will have to be performed to obtain accurate and precise descriptions of the ruthenium fluoride behavior, facilitating both MSR management and future research.

References

[1] Juhn, P.E.; Kupitz, J., "Nuclear Power beyond Chernobyl: A changing international perspective," International Atomic Energy Agency, 1 1996. [Online]. Available: https://www.iaea.org/sites/default/files/publications/magazines/bulletin/bull38-1/38104780209.pdf. [Accessed 28 5 2018].

[2] World Nuclear Association, "Molten Salt Reactors," 8 2017. [Online]. Available: http://world-nuclear.org/information-library/current-and-future-generation/molten-salt-reactors.aspx. [Accessed 31 5 2018].

[3] Compere, E.L.; Kirslis, S.S.; Bohlmann, E.G.; Blankenship, F.F.; Grimes, W.R., "Fission Product Behavior in the Molten Salt Reactor Experiment," US Department of Commerce, Springfield, VA, 1975.

[4] Baes Jr., C.F., *J.Nuc.Mater.,* vol. 51, no. 1, pp. 149-62, 1974.

[5] Olander, D., *J.Nuc.Mater.,* no. 300, pp. 270-72, 2002.

[6] Baes Jr., C.F., "Equilibrium Pressures of Noble-Metal Fluorides under MSRE conditions," in *Reactor Chemistry Division Annual Progress Report ORNL-4076*, Springfield, VA, US Department of Commerce, 1967.

[7] Freestone, N.Ph., "The Chemistry of Ruthenium Fluorides: Investigation of Methods of Removal of Traces of RuF5 from mixtures of Volatile Fluorides," in *Purification of Uranium Hexafluoride by Non-Aqueous Means*, Leicester, UMI Dissertation Publishing, 1987, pp. 203-43.

[8] Claassen, H.H.; Selig, H.; Malm, J.G.; Chernick, C.L.; Weinstock, B., *J.Am.Chem.Soc.,* vol. 83, pp. 2390-91, 1961.

[9] Hildebrand, D.L.; Lau, K.H., *J.Chem.Phys,* vol. 89, pp. 5825-28, 1988.

[10] Page, E.M.; Rice, D.A.; Almond, M.J.; Hagen, K.; Volden, H.V.; Holloway, J.H.; Hope, E.G., *Inorg.Chem.,* vol. 32, pp. 4311-16, 1993.

[11] Hargittai, M., *Chem.Rev.,* vol. 100, pp. 2233-2301, 2000.

[12] Jarid, A.; Aaid, M.; Legoux, Y.; Merini, J.; Loudet, M.; Gonbeau, D.; Pfister-Guillouzo, G., *Chem.Phys.,* vol. 150, no. 3, pp. 353-60, 1991.

[13] Nikitin, M.I.; Zbezheva, S.G., *High Temp.,* vol. 50, no. 2, pp. 186-93, 2012.

[14] Siegbahn, P.E.M., *Theor.Chim.Acta,* vol. 86, pp. 219-28, 1993.

[15] Siegbahn, P.E.M., *Theor.Chim.Acta,* vol. 87, pp. 441-52, 1994.

[16] Galkin, N.P., Main Properties of Inorganic Fluorides. Handbook (Russian), Moscow: Atomisdat, 1976.

[17] Drews, T.; Supel, J.; Hagenbach, A.; Seppelt, K., *Inorg.Chem.,* vol. 45, no. 9, pp. 3782-88, 2006.

[18] Porte, H.A.; Greenberg, E.; Hubbard, W.N., *J.Phys.Chem.,* vol. 69, no. 7, pp. 2308-10, 1965.

[19] Cramer, C.J., Essentials of Computational Chemistry. Theories and Models, 2nd ed., Chichester: John Wiley & Sons Ltd., 2004.

[20] Stephens, P.J.; Devlin, F.J.; Chabalowski, C.F.; Frisch, M.J., *J.Phys.Chem.,* vol. 98, p. 623, 1994.

[21] Becke, A.D., *Phys.Rev.A,* vol. 38, p. 3098, 1988.

[22] Lee, C.; Yang, W.; Parr, R.G., *Phys.Rev.B,* vol. 117, p. 785, 1988.

[23] Ochterski, J. W., "Vibrational Analysis in Gaussian," 29 10 1999. [Online]. Available: https://gaussian.com/vib/. [Accessed 7 7 2018].

[24] Ochterski, J.W., "Thermochemistry in Gaussian," 2 6 2000. [Online]. Available: https://gaussian.com/wp-content/uploads/dl/thermo.pdf. [Accessed 28 6 2018].

[25] Capelli, E.; Konings, R.J.M., *J.Fluor.Chem.,* vol. 208, pp. 55-64, 2018.

[26] CALPHAD, [Online]. Available: http://www.calphad.org/. [Accessed 18 7 2018].

[27] "Gaussian 09, Rev. B.01," Gaussian Inc., Wallingford, CT, 2010.

[28] Institute for Theroretical Chemistry, "Energy-consistent Pseudopotentials of the Stuttgart/Cologne Group," University of Cologne, 10 7 2014. [Online]. Available: http://www.tc.uni-koeln.de/PP/clickpse.en.html. [Accessed 27 11 2017].

[29] National Instituite of Standards and Technology, "NIST-JANAF Thermochemical Tables," US Department of Commerce, [Online]. Available: https://janaf.nist.gov/. [Accessed 28 6 2018].

[30] Wagman, D.D.; Evans, W.H.; Parker, V.B; Schumm, R.H.; Halow, I.; Balley, S.M.; Churney, K.L.; Nuttal, R.L., The NBS Tables of Chemical Thermodynamic Properties, American Chemical Society, 1982.

[31] Moore, C.E., Atomic Energy Levels as obtained from the Analyses of Optical Spectra, vol. III, Washington, DC: US National Institute of Standards and Technology, 1958 (rev. 1971).

[32] Weinstock, B.; Goodman, G.L., *Adv.Chem.Phys,* vol. 9, p. 169, 1965.

[33] Barin, I.; Knacke, O.; Kubaschewski, O., Thermochemical Properties of Inorganic Substances, Berlin: Springer-Verlag, 1977.

[34] Holloway, J.H.; Peacock, R.D., *J.Chem.Soc.,* no. 0, pp. 527-30, 1963.

[35] M. Hargittai, „Molecular Structure of Metal Halides," *Chem.Rev.,* vol. 100, pp. 2233-2301, 2000.

A. Worked-out Contributions

Rotational Contributions

For linear molecules, the rotational thermodynamic contributions for linear molecules are

$$\begin{gathered} S_r(T) = R\left(\ln\frac{q_r}{N} + T\left(\frac{1}{T}\right)\right) = R\left(\ln\left(\frac{1}{\sigma N}\left(\frac{T}{\Theta_r}\right)\right) + 1\right) \\ (H(T) - H^0)_r = RT^2\left(\frac{1}{T}\right) = RT \\ C_{P_r} = R \end{gathered} \tag{A1}$$

For a general, non-linear molecule (Eq. 19), rotation contributes like

$$\begin{gathered} S_r(T) = R\left(\ln\frac{q_r}{N} + T\left(\frac{3}{2T}\right)\right) = R\left(\ln\left(\frac{\sqrt{\pi}}{\sigma N}\left(\frac{T^{3/2}}{\sqrt{\Theta_{r,x}\Theta_{r,y}\Theta_{r,z}}}\right)\right) + \frac{3}{2}\right) \\ (H(T) - H^0)_r = RT^2\left(\frac{3}{2T}\right) = \frac{3}{2}RT \\ C_{P_r}(T) = \tfrac{3}{2}R \end{gathered} \tag{A2}$$

which comes down to contributions of $RT/2$ to the enthalpy and of $R/2$ to the heat capacity per degree of freedom [24]. In Table 6, this is clearly visible for the heat capacity.

Vibrational Contributions

The complexity of the total partition function (product of all *K* Eqs. 20) results in more difficult calculations for the thermodynamic consequences of vibrational motion, the final results of which [24] are

$$\begin{gathered} S_v(T) = R\sum\nolimits_K\left(\frac{\Theta_{v,K}/T}{e^{\Theta_{v,K}/T} - 1} - \ln\left(1 - e^{-\Theta_{v,K}/T}\right)\right) \\ (H(T) - H^0)_v = R\sum\nolimits_K \Theta_{v,K}\left(\frac{1}{2} + \frac{1}{e^{\Theta_{v,K}/T} - 1}\right) \\ C_{P_v} = R\sum\nolimits_K e^{\Theta_{v,K}/T}\left(\frac{\Theta_{v,K}/T}{e^{-\Theta_{v,K}/T} - 1}\right)^2 \end{gathered} \tag{A3}$$

Electronic Contributions

When given the electronic states as input, *MoTher* calculates the electronic contributions to the thermodynamics:

$$\begin{gathered} S_e = R\left(\ln\frac{\sum_n \omega_n e^{-\epsilon_n/k_BT}}{N} + T\left(\frac{\sum_n \frac{\omega_n\epsilon_n e^{-\epsilon_n/k_BT}}{k_BT^2}}{\sum_n \omega_n e^{-\epsilon_n/k_BT}}\right)\right) = R\left(\ln\frac{q_e}{N} + \frac{\sum_n \omega_n\epsilon_n e^{-\epsilon_n/k_BT}}{q_e k_BT}\right) \\ (H(T) - H^0)_e = RT^2\left(\frac{\sum_n \frac{\omega_n\epsilon_n e^{-\epsilon_n/k_BT}}{k_BT^2}}{\sum_n \omega_n e^{-\epsilon_n/k_BT}}\right) = N_A\left(\frac{\sum_n \omega_n\epsilon_n e^{-\epsilon_n/k_BT}}{q_e}\right) \\ C_{P_e} = \frac{N_A}{k_BT^2}\frac{\left(\sum_n \omega_n e^{-\epsilon_n/k_BT}\right)\left(\sum_n \omega_n {\epsilon_n}^2 e^{-\epsilon_n/k_BT}\right) - \left(\sum_n \omega_n\epsilon_n e^{-\epsilon_n/k_BT}\right)^2}{\left(\sum_n \omega_n e^{-\epsilon_n/k_BT}\right)^2} \end{gathered} \tag{A4}$$

where *n* effectively runs over occupied electronic levels only, because the exponent approaches zero for the higher energetic levels.

B. Heat Capacities relationship

There is a discrete distinction between the isochoric heat capacity C_V and the isobaric heat capacity C_P. They are defined as

$$C_V = \left(\frac{\partial E}{\partial T}\right)_{N,V} \quad \text{and} \quad C_P = \left(\frac{\partial H}{\partial T}\right)_{N,P} \tag{B1}$$

It is immediately evident where the difference comes from. First of all, as the names clarify, the isochoric system operates in a constant volume, allowing the pressure to vary, whereas the isobaric system operates under constant pressure, while it may vary its volume. Additionally, the work that the system does by variation of its volume is taken into account in the isobaric heat capacity, as it is calculated from $H = E + PV$ rather than from just E. The heat capacities reported, those that *MoTher* computes, are the isobaric heat capacities, while *Gaussian*, as outlined in its whitepaper [24], calculates the isochoric heat capacities.

For ideal gases, however, there is also a fairly simple relationship between these two heat capacities. In general, it can be derived from thermodynamics that the difference between the two heat capacity expressions is

$$C_P - C_V = T\left(\frac{\partial P}{\partial T}\right)_{N,V}\left(\frac{\partial V}{\partial T}\right)_{N,P} \tag{B2}$$

From the ideal gas law, it is clear that

$$P = \frac{nRT}{V}, \qquad \left(\frac{\partial P}{\partial T}\right)_{N,V} = \frac{nR}{V} \tag{B3}$$

$$V = \frac{nRT}{P}, \qquad \left(\frac{\partial V}{\partial T}\right)_{N,P} = \frac{nR}{P} \tag{B4}$$

Division by *N* = 1 mol (i.e. *n* = 1) obtains intensive quantities, and substitution into Eq. B2 yields

$$C_{P,m} - C_{V,m} = T\frac{R}{V_m}\frac{R}{P} = \left(\frac{RT}{V_m}\right)\frac{R}{P} = P\frac{R}{P} = R \tag{B5}$$

Of course, this relationship is valid only for the full heat capacities, and not for all of its contributing components singularly.

C. Exemplary input files

Exemplary Gaussian *input file*

RuF_5 (D_{3h}), multiplicity 4. Geometry is followed by basis sets and pseudopotentials.

```
%chk=RuF5.chk
%nprocshared=8
%Mem=500MB
# B3LYP/gen pseudo=read opt freq pop=none

RuF5

0 4
Ru
F 1 r2
F 1 r1 2 a1
F 1 r1 2 a1 3 a2 1
F 1 r1 2 a1 4 a2 1
F 1 r2 2 a3 4 a1 1

r1=1.85
r2=1.80
a1=90.
a2=120.
a3=180.

F  0
cc-pVTZ
****
Ru 0
S 3 1.00
7.9365700 -1.1196656
5.9842450 1.4453293
4.8822200 0.6261653
S 1 1.00
1.1446240 1.0
S 1 1.00
0.5230170 1.0
S 1 1.00
0.1175730 1.0
S 1 1.00
0.0480500 1.0
S 1 1.00
0.0160000 1.0
P 2 1.00
3.7546090 -4.7226565
2.9165710 4.9909084
P 2 1.00
1.0486750 0.7285467
0.5073200 0.3039043
P 1 1.00
0.2673980 1.0
P 1 1.00
0.0697480 1.0
P 1 1.00
0.0229270 1.0
D 4 1.00
6.0099130 -0.0327160
2.1042800 0.2657392
0.9215000 0.4812398
0.3885980 0.4099778
D 1 1.00
0.1528360 1.0
D 1 1.00
0.0510000 1.0
F 1 1.00
1.6660000 1.0
F 1 1.00
0.4780000 1.0
G 1 1.00
1.0570000 1.0
****

Ru 0
ECP28MWB 4 28
G-Komponente
1
2 1.000000 0.000000
S-G
2
2 11.105269 209.822971
2 5.414745 30.654726
P-G
2
2 9.771271 146.336182
2 5.073991 24.127877
D-G
2
2 7.671423 67.515897
2 4.136565 9.870104
F-G
2
2 11.360000 -28.340616
2 5.680000 -4.944629
```

Exemplary MoTher *input file*

Optimized structure of RuF_2, mentioning consecutively the number of atoms and the rotational symmetry number σ, the atomic energy levels, the 3D moment of inertia and the vibrational modes.

```
RuF2
  3  2.
  6
   0.0    1
1158.8    1
1826.3    1
2266.3    1
2476.0    1
27162.8    1
  2.214420-45
 3
  141.5      2
  609.5      1
  680.4      1
 0
 -000000  2
Ru  1.0
F2  1.0
```